Model-based analysis of dispersion curves using chirplets

Helge Kuttig[a)]
School of Civil and Environmental Engineering, Georgia Institute of Technology, Atlanta, Georgia 30332-0355

Marc Niethammer
Department of Psychiatry, Brigham and Women's Hospital, Harvard Medical School, Boston, Massachusetts 02215

Stefan Hurlebaus
Zachry Department of Civil Engineering, Texas A&M University, College Station, Texas 77843-3136

Laurence J. Jacobs[b)]
School of Civil and Environmental Engineering and G. W. Woodruff School of Mechanical Engineering, Georgia Institute of Technology, Atlanta, Georgia 30332

(Received 18 November 2005; revised 23 January 2006; accepted 24 January 2006)

Time-frequency representations, like the spectrogram or the scalogram, are widely used to characterize dispersive waves. The resulting energy distributions, however, suffer from the uncertainty principle, which complicates the allocation of energy to individual propagation modes (especially when the dispersion curves of these modes are close to each other in the time-frequency domain). This research applies the chirplet as a tool to analyze dispersive wave signals based on a dispersion model. The chirplet transform, a generalization of both the wavelet and the short-time Fourier transform, enables the extraction of components of a signal with a particular instantaneous frequency and group delay. An adaptive algorithm identifies frequency regions for which quantitative statements can be made about an individual mode's energy, and employs chirplets (locally adapted to a dispersion curve model) to extract the (proportional) energy distribution of that single mode from a multimode dispersive wave signal. The effectiveness of this algorithm is demonstrated on a multimode synthetic Lamb wave signal for which the ground-truth energy distribution is known for each mode. Finally, the robustness of this algorithm is demonstrated on real, experimentally measured Lamb wave signals by an adaption of a correlation technique developed in previous research. [DOI: 10.1121/1.2177587]

PACS number(s): 43.35.Cg, 43.60.Hj [YHB] Pages: 2122–2130

I. INTRODUCTION

Ultrasonic waves are used for material characterization in many structural health monitoring and nondestructive evaluation applications. Guided ultrasonic waves (such as Lamb waves) are particularly effective in interrogating large structural components, because guided waves propagate far distances (when compared to body waves); see Chimenti[1] for details. Unfortunately, the dispersive nature of these guided waves complicates their analysis in the time-domain, so time-frequency representations (TFRs) are often employed to better interpret a guided wave signal. Time-frequency analysis represents the frequency content of a time-domain signal over time, and is thus ideally suited for the analysis of dispersive waves. Niethammer *et al.*[2] demonstrated the effectiveness of using TFRs for Lamb waves, while Hurlebaus *et al.*[3,4] describe several applications for crack detection and localization in a plate using TFRs such as the spectrogram and the scalogram.

In 1991, Mann *et al.*[5] coined the term "chirplet transformation" for a new TFR, a generalization of the spectrogram and scalogram with additional degrees of freedom for time and frequency shear. While the chirplet transform allows for the decomposition of time-domain signals into well-localized components (time-frequency atoms) with a constant chirp rate (that is, linearly changing instantaneous frequency), the resulting representation is of dimension five. This complicates the visualization, computation, and interpretation of a transformed signal. In order to apply the chirplet transform to signals containing chirplike components, such as, Doppler radar signals, electroencephalographies (EEGs), bird voices or bat sonar signals, researchers reduce the problem's complexity by considering only subspaces[6,7] of the five-dimensional parameter space or by employing a matching pursuit algorithm to search for ridges in a coarsely discretized parameter space.[8]

Hong *et al.*[9] utilize a dispersion-based short-time Fourier transform (a chirplet transform) for the analysis of dispersion curves from guided wave signals. In contrast, the objective of the current research is to establish a model-based chirplet analysis of dispersive waves grounded in the theory developed by Mann,[5] and then to investigate the quantitative behavior of the proposed method for the analysis of dispersion

[a)]Current address: Institute of Applied and Experimental Mechanics, University of Stuttgart, Pfaffenwaldring 9, 70569 Stuttgart, Germany.
[b)]Electronic mail: laurence.jacobs@ce.gatech.edu

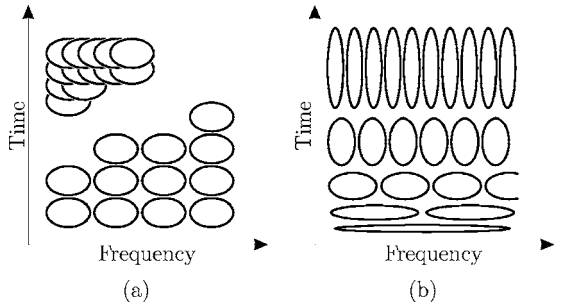

FIG. 1. Tiling of the time-frequency plane by time-frequency representations. Each ellipse represents one time-frequency atom. (a) Spectrogram. (b) Scalogram.

curves. The dispersion curve model used in this study is the Rayleigh-Lamb equations, which describes wave propagation in platelike structures. The proposed algorithm is first validated on a synthetic signal for which the ground-truth energy distribution is known for each mode. Finally, the robustness of this algorithm is demonstrated on real, experimentally measured Lamb wave signals by an adaption of the correlation technique developed in previous research.[4,10,11]

II. REVIEW OF TFRS FOR GUIDED WAVES

The dispersive nature of Lamb waves (guided ultrasonic waves in plates) means that the frequency content of a measured Lamb wave signal varies as a function of time. A simple time- or frequency-domain representation of such a dispersive signal does not (individually) localize the energy content of a Lamb wave in the time-frequency domain. So, more advanced tools such as TFRs, are needed for the comprehensive analysis of these dispersive signals. One such TFR, the short-time Fourier transform (STFT), C_x^{stft}, is calculated for a signal $x(t)$ as follows:[12]

$$C_x^{\mathrm{stft}}(t,\omega) = \int_{-\infty}^{+\infty} x(\tau) h(\tau - t) e^{-i\omega\tau} d\tau, \tag{1}$$

where $h(t)$ is a window function. The square modulus of the STFT is called the spectrogram $P^{\mathrm{sp}}(t,\omega) = |C_x^{\mathrm{stft}}(t,\omega)|^2$ and yields the energy density of the signal x in the time-frequency domain.

All TFRs suffer from the uncertainty principle,[13] so the resulting time-frequency values do not necessarily correspond to the exact energy distribution of a signal in the time-frequency domain; TFRs based on smoothing kernels (like the spectrogram and scalogram) result in smoothed versions of the exact energy distribution.[14] The extent of the smoothing depends on the smoothing kernel (the window function) employed. For a spectrogram using a Gaussian window function

$$h(t) = \frac{1}{\sqrt[4]{\pi s^2}} \exp\left[-\frac{1}{2}\left(\frac{t - t_0}{s} \right)^2 \right],$$

this smoothing (averaging) effect is minimized, and the regions of averaging can be approximately visualized by ellipses of the same size and shape as shown in Fig. 1(a).

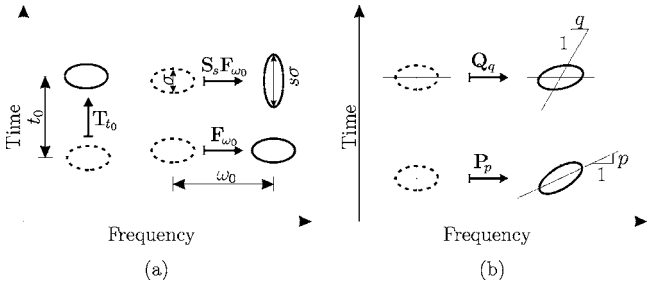

FIG. 2. Representation of time-frequency atoms of a TFR. (a) The generalization of the STFT and wavelet transforms by introducing the operators $\mathbf{T}_{t_0}$, $\mathbf{F}_{\omega_0}$, and $\mathbf{S}_s$ which allows arbitrary time and frequency shifts, and scale. (b) Modulation with a chirp in the time domain ($\mathbf{Q}_q$) shears the time-frequency atom in the frequency direction, modulation with a chirp in the frequency-domain ($\mathbf{P}_p$) shears in the time direction. The shear parameters p and q determine the slope of the semiaxes of the chirplet atom ellipses.

Other TFRs result in different tilings of the time-frequency domain; consider, for example, the wavelet transform, C_x^{wt} of a signal $x(t)$,

$$C_x^{\mathrm{wt}}(t,s) = \int_{-\infty}^{+\infty} x(\tau) \frac{1}{\sqrt{s}} \psi^*\left(\frac{\tau - t}{s} \right) d\tau, \tag{2}$$

where s is a dilatation and t is a shift parameter, which scale and shift the mother wavelet $\psi(t)$ and $(\cdot)^*$ denotes the complex conjugate. The energy density $P^{\mathrm{wt}}(t,s) = |C_x^{\mathrm{wt}}(t,s)|^2$ is called the scalogram and again localizes the energy of a signal in the time-frequency domain under the restrictions of the uncertainty principle, yielding to a tiling of the time-frequency domain as shown in Fig. 1(b).

III. THE CHIRPLET TRANSFORM

Both the STFT and the wavelet transform result from the inner multiplication of the time function under consideration with a time-frequency atom, $g(t)$

$$C_x = \int_{-\infty}^{+\infty} x(\tau) g^*(\tau) d\tau. \tag{3}$$

This time-frequency atom is obtained from the window function by either shifting it in the time and frequency directions (STFT), or with a time shift and scale (wavelet transformation); a comparison is shown in Fig. 2(a).

By introducing the time and frequency shift operators $\mathbf{T}_{t_0}$ and $\mathbf{F}_{\omega_0}$ and the scale operator $\mathbf{S}_s$ as defined in Table I, a generalized three-dimensional TFR is written as

$$C_x = \int_{-\infty}^{+\infty} x(\tau) g^*_{t_0,\omega_0,s}(\tau) d\tau \tag{4}$$

with

$$g_{t_0,\omega_0,s}(t) = \mathbf{T}_{t_0} \mathbf{F}_{\omega_0} \mathbf{S}_s h(t). \tag{5}$$

Mann[7] uses this framework and expands it by two additional operators to formulate the chirplet transform.

(1) Frequency shear: The time-frequency atom is multiplied by a harmonic function of linearly changing frequency (a "chirp" function)

TABLE I. Operations for time-frequency atoms for the chirplet transform, k_p is a complex scaling factor.

Operation		Corresponding coordinate transformation $(t,\omega)\rightarrow(\bar{t},\bar{\omega})$	
Time shift $\mathbf{T}_{t_0}$	$\mathbf{T}_{t_0}h(t)=h(t-t_0)$	$\bar{t}=t-t_0$	$\bar{\omega}=\omega$
Frequency shift $\mathbf{F}_{\omega_0}$	$\mathbf{F}_{\omega_0}h(t)=e^{i\omega_0 t}h(t)$	$\bar{t}=t$	$\bar{\omega}=\omega-\omega_0$
Scaling $\mathbf{S}_s$	$\mathbf{S}_s h(t)=\frac{1}{\sqrt{s}}h\left(\frac{t}{s}\right)$	$\bar{t}=\frac{t}{s}$	$\bar{\omega}=s\omega$
Frequency shear $\mathbf{Q}_q$	$\mathbf{Q}_q h(t)=h(t)\exp[iq/2t^2]$	$\bar{t}=t$	$\bar{\omega}=\omega-qt$
Time shear $\mathbf{P}_p$	$\mathbf{P}_p h(t)=k_p\exp\left[-i\frac{1}{2q}t^2\right]\times h(t)$	$\bar{t}=t-p\omega$	$\bar{\omega}=\omega$

$$g_q(t)=\mathbf{Q}_q h(t)=h(t)\exp\left[i\frac{q}{2}t^2\right]. \tag{6}$$

This modulation with a time-dependent frequency results in a shear $\mathbf{Q}_q$ of the time-frequency atom in the frequency direction as shown in Fig. 2(b). The time-frequency atom is now concentrated along a line with slope $1/q$.

(2) Time shear: The corresponding multiplication of a chirp function with the time-frequency atom in the frequency-domain (according to a convolution in the time-domain) constitutes the dual operation to the frequency shear, the shear $\mathbf{P}_p$ in the time direction

$$g_p(t)=\mathbf{P}_p h(t)=\sqrt{\frac{2\pi}{p}}\exp\left[i\left(-\frac{1}{2q}t^2+\frac{\pi}{4}\right)\right]\times h(t). \tag{7}$$

The effect of this operation is shown in Fig. 2(b); one semiaxis of the time-frequency atom has the slope p. The complex scaling factor $\sqrt{(2\pi/p)}\exp[i\pi/4]$ results from the transformation from the frequency domain.

Using these five operations, time-frequency atoms can be translated, scaled and sheared in the time-frequency domain. Each operation specifies a linear or affine coordinate transformation in the time-frequency domain. The mapping equations for the transformations are listed in Table I. A time-frequency atom transformed like this is called a "chirplet atom" or, in short, "chirplet" $g_{t_0,\omega_0,s,q,p}(t)$

$$g_{t_0,\omega_0,s,q,p}(t)=\mathbf{T}_{t_0}\mathbf{F}_{\omega_0}\mathbf{S}_s\mathbf{Q}_q\mathbf{P}_p h(t). \tag{8}$$

The chirplet transform C_x^{ct} as defined by Mann *et al.*[5] is obtained by the inner multiplication of a chirplet atom with a time-domain signal

$$C_x^{\mathrm{ct}}(t_0,\omega_0,s,q,p)=\int_{-\infty}^{+\infty}x(\tau)g^*_{t_0,\omega_0,s,q,p}(\tau)d\tau. \tag{9}$$

The operators just described are not commutative, and interchanging two of them generally results in a phase shift of the chirplet. This will not be discussed further, as only the magnitudes of chirplet transforms are processed in this research.

Signal components which are concentrated in the time-frequency domain at a location specified by the parameters t_0, ω_0, s, q, and p can be extracted by performing a chirplet transform. Analogous to the spectrogram and scalogram, one defines the energy distribution

$$P^{\mathrm{ct}}(t_0,\omega_0,s,q,p)=|C_x^{\mathrm{ct}}(t_0,\omega_0,s,q,p)|^2. \tag{10}$$

For a given basic window, this results in a five-dimensional representation which is difficult to visualize. So instead of calculating the entire five-dimensional space, one often confines oneself to a plane spanned by two parameters in order to visualize the time-frequency content (like (t_0,ω_0) for the spectrogram).

Note that another approach is to decompose a signal into the chirplet's base, e.g., an algorithm to find local maxima in the five-dimensional space.[8] Finally, an alternative formulation of chirplets that is based on the Wigner-Ville distribution is presented by Baraniuk *et al.*[6]

IV. LAMB WAVE ENERGY ASSIGNMENT TO MODES

Lamb waves are multimode signals, so it is of great practical interest to develop a quantitative description of the energy distribution of the signal amongst the individual Lamb modes. The dispersion relationship (the relationship between wavenumber and frequency, which can be converted to the time-frequency domain) of guided Lamb waves propagating in a homogenous, isotropic plate of thickness $2h$ is described by the Rayleigh-Lamb equations[15]

$$\frac{\tan(\tilde{q}h)}{\tan(\tilde{p}h)}=-\frac{4k^2\tilde{p}\tilde{q}}{(\tilde{q}^2-k^2)^2}, \tag{11a}$$

$$\frac{\tan(\tilde{q}h)}{\tan(\tilde{p}h)}=-\frac{(\tilde{q}^2-k^2)^2}{4k^2\tilde{p}\tilde{q}}, \tag{11b}$$

where k is the wavenumber ($k=2\pi/\lambda$, where λ is wavelength), ω is angular frequency ($\omega=2\pi f$, where f is frequency in Hz), and

$$\tilde{p}^2=\frac{\omega^2}{c_{\mathrm{L}}^2}-k^2,\quad \tilde{q}^2=\frac{\omega^2}{c_{\mathrm{T}}^2}-k^2. \tag{12}$$

c_L and c_T are the longitudinal and transverse wave speeds, respectively.

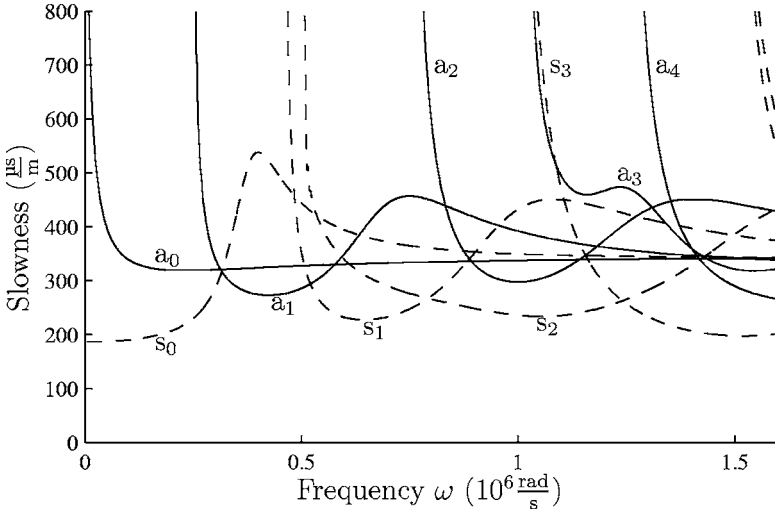

FIG. 3. Theoretical solution of Raleigh-Lamb equation for an aluminum 3003 plate of thickness 0.99 mm in the slowness-frequency domain. s_i denotes symmetric, a_i denotes antisymmetric Lamb modes.

Solutions of these equations, the dispersion curves, are plotted in Fig. 3 for an aluminum plate of thickness 0.99 mm. Each propagation mode in Fig. 3 corresponds to a single line, with modes numbered in order of the lowest frequency as they appear, and s_i and a_i denotes modes with symmetric and antisymmetric displacement profiles (with respect to the axis of propagation), respectively. These results are shown in the slowness-frequency domain, where slowness (sl_e) is defined as the reciprocal value of the group velocity. This representation is a normalization to the propagation (source-to-receiver) distance (d), where $sl_e = t/d$.

In typical structural health and nondestructive evaluation applications of guided ultrasonic waves, the displacement or velocity of a particle on the surface of a structural component is measured. In general, this displacement (or particle velocity) contains energy contributions from all the propagating modes (a superposition of all these modes) and it is difficult (if not impossible) to separate the contributions from each individual mode in a measured signal. The ability to accurately separate these individual modal energy contributions from a measured, multimode Lamb wave would significantly enhance current structural health and nondestructive evaluation applications. This research uses the chirplet to accurately separate these individual modal energy contributions from a multimode Lamb wave signal by using the Rayleigh-Lamb dispersion model given by Eq. (11)—the dispersion relationship shown in Fig. 3 is assumed to be known.

Consider a synthetically generated Lamb wave signal (developed following Refs. 16 and 17) where the exact energy distribution for each individual mode is known. This synthetic time-domain signal is an "ideal measurement" of a guided Lamb wave in an aluminum plate of thickness 0.99 mm. This synthetic signal represents ground-truth; the excitability of each mode is known, so it is possible to absolutely calculate the energy content of each of the propagation modes.

Note that the energy of a Lamb wave mode is proportional to the square of its displacement, but the constant of proportionality is mode and frequency dependent. Therefore, it is not prudent to develop an absolute ratio of the energies of the individual Lamb modes. Instead, consider the ratio of the surface displacements of two Lamb wave modes; the square root of the chirplet energy distribution defined by Eq. (10) is proportional to displacement (as is the square root of the spectrogram). This paper concentrates on the s_0 and a_0-modes—these two lowest modes carry most of the energy for the example under consideration—and will present the ratio of the out-of-plane displacements of mode s_0 over a_0, which will be referred to as the "mode displacement ratio." While not equal to a mode energy ratio, this representation will allow for the source-independent presentation of the relative "energy" distributions of each individual mode, which can be compared to the corresponding theoretical (ground-truth) values.

A. Calculating the mode displacement ratio using the spectrogram

First, consider the results when using the spectrogram to calculate the mode displacement ratio of this synthetic (time-domain) Lamb wave signal. A synthetic Lamb wave is generated for a propagation distance of 90 mm and a sampling frequency of 100 MHz (shown in the time-domain in Fig. 4) and is then operated on with a 1024-point Hanning window to calculate the spectrogram shown in Fig. 5 [plus the theoretical dispersion curves calculated using Eq. (11)]. Note that the time-domain signal in Fig. 4 contains the ten lowest modes, represents out-of-plane displacement, and has been highpass filtered at 0.3 MHz. Most of the energy of the spectrogram is localized near the theoretical dispersion curves, and it is a reasonable next step to calculate the (proportional) energy of the individual modes by simply using the magnitude values of the spectrogram—the amplitudes in the contour plot of Fig. 5 at each slowness-frequency position associated with the theoretical dispersion curves. The results of this operation (mode displacement ratio of s_0 over a_0) are plotted as a dotted line in Fig. 6, along with the known theoretical curve (as a solid gray line). The mode displacement ratio values calculated with the spectrogram are only close to the theoretical values in certain frequency regions; this poor agreement is primarily due to the uncertainty principle, since the spectrogram calculates the energy at a particular slowness-frequency (normalized time-frequency) location by taking an average over a certain region in the

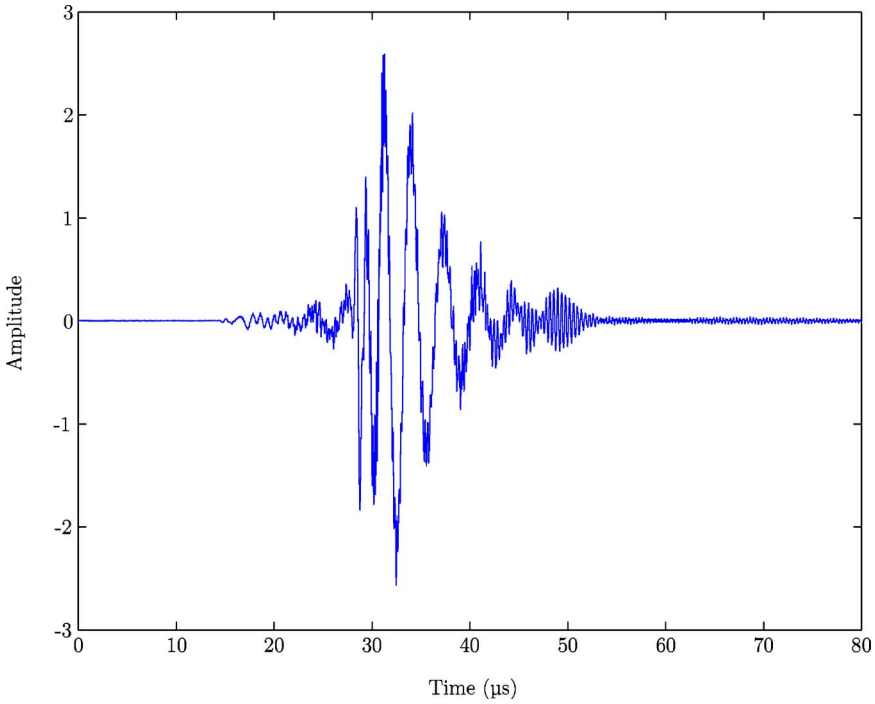

FIG. 4. (Color online) Synthetic time-domain signal, out-of-plane displacement, propagation distance $d=90$ mm.

slowness-frequency domain. This behavior is illustrated in Fig. 7(a), and note that when evaluating the spectrogram for one dispersion curve, contributions from its neighboring or intersecting dispersion curves are often inadvertently included.

B. Calculating the mode displacement ratio using chirplets

It is possible to improve the spectrogram results presented in Fig. 6 by instead using the additional degrees of freedom of the chirplet transform, combined with the dispersion model of Eq. (11). By using this dispersion relationship model, it is possible to adapt the shape of a chirplet to fit the known group delay of each propagation mode. This group delay describes which frequencies are present in a Lamb wave signal at a particular time, and is proportional to the slowness representation of a Lamb wave's dispersion curves. Using this procedure, the (proportional) energy of a particular propagation mode is extracted from a multimode signal with chirplets which are parametrized to be concentrated on the mode's dispersion curve in the slowness-frequency domain. This is accomplished by shifting chirplets onto the dispersion curve, and then shearing them to locally match the slope of the dispersion curve. The chirplet parameters t_0 and ω_0 are determined by the coordinates of the dispersion curve, and the parameter p equals the slope of the dispersion curve at the point (t_0, ω_0).

While the time-frequency atoms of the spectrogram-based energy analysis only match the position of the dispersion curve, a chirplet is concentrated on a straight line with the same rate as the dispersion curve. This is visualized in Fig. 7(b). As a result, the chirplet-based energy analysis matches the group delay of the signal as a first-order approximation (in contrast to the zeroth-order approximation of the spectrogram). Either a time or a frequency shear operator can be used to realize this matching of the chirplet onto the dis-

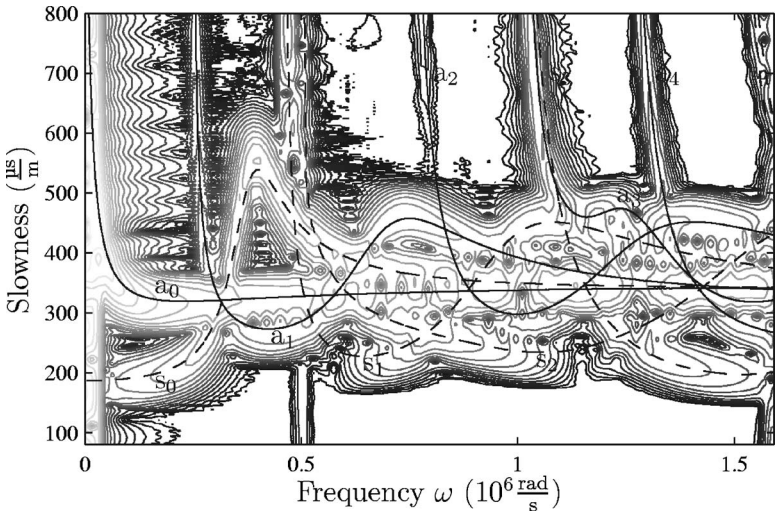

FIG. 5. Spectrogram of the synthetic time signal with theoretical dispersion curves.

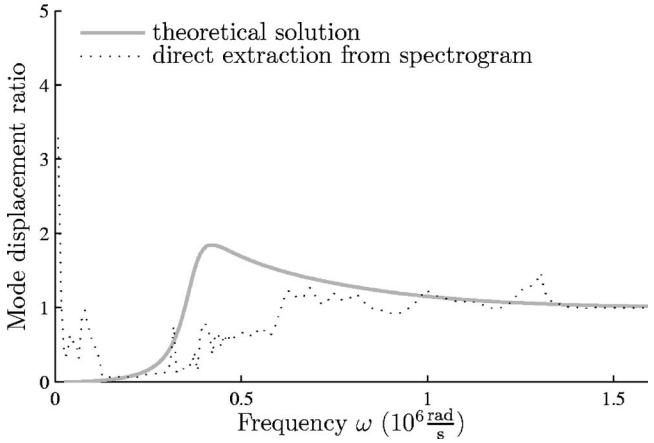

FIG. 6. Mode displacement ratio of mode s_0 over mode a_0, obtained by directly evaluating the spectrogram at the dispersion curves. Compare to the theoretical displacement ratio (solid gray line).

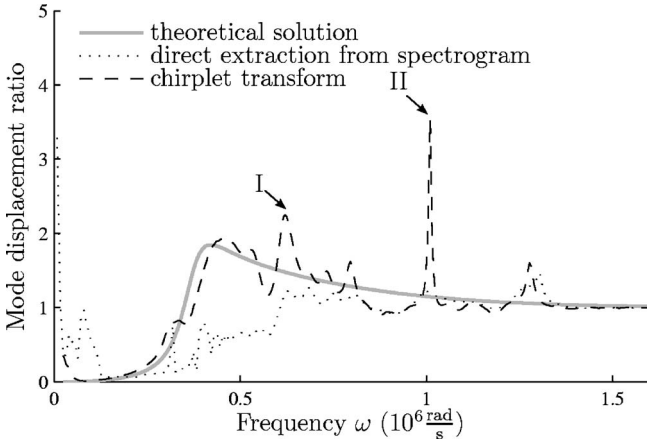

FIG. 8. Mode displacement ratio of mode s_0 over mode a_0, obtained by using time sheared chirplets which are concentrated along the dispersion curves of the modes. Compare to theoretical displacement ratio (solid gray line). (I) and (II) denote large discrepancies of the chirplet calculations and the theoretical displacement ratio, caused by the intersection of the dispersion curves of modes s_0 and a_1 (I), and by the proximity of modes s_0 and a_0 (II), respectively.

persion curve, since each operation shears one of the semiaxes of the time-frequency region of averaging. Since the dispersion curves are functions of frequency, only the time shear operation is used in this research to avoid singularities. An extension of the chirplet transform to shear operations of higher order allows for an adaption of a chirplet to dispersion curves of order higher than one, but does not show significant improvements in the accuracy of the mode displacement ratio calculations,[18] so this research only applies first order shear, and does not use one of the five possible chirplet operations (degrees of freedom).

This chirplet transformation (using chirplets which are concentrated along the dispersion curves by shearing them in the time direction) is used to calculate the mode displacement ratio of s_0 over a_0, which is compared to the theoretical and spectrogram-based results in Fig. 8.

It is important to note that the main advantage of the chirplet over the spectrogram (and scalogram) is this additional control over the shape, location, and orientation of the time-frequency atoms. All these TFRs will provide an average energy over a region in the time-frequency domain, but the chirplet provides additional degrees of freedom to control this averaging region. As a result, the chirplet should be better in resolving closely spaced modes.

C. Adaptive chirplets

Inspection of the chirplet transform results in Fig. 8 shows that the recovered mode displacement ratio is a better match to the theoretical solution than the spectrogram-based results. However, there is poor agreement between the chirplet-based and theoretical solution in the frequency ranges where two dispersion curves intersect (compare to the dispersion curves of the plate shown in Figs. 3 and 10). The regions of greatest discrepancy in Fig. 8 are indicated by (I) and (II), and occur at frequencies where the s_0-mode's dispersion curve intersects with the dispersion curve of the a_1 mode, or where the s_0- and a_0-modes are close to each other. A large portion of those modes' energy must have been improperly assigned to the s_0-mode in these frequency ranges using this procedure.

This error can be addressed by exploiting another (a fourth) degree of freedom of the chirplet transform—the scale s. An improved, adaptive chirplet analysis algorithm can also account for a mode's intersections (and closeness) to its neighboring modes, in addition to its own dispersion curve model. As in the previous chirplet algorithm, chirplets

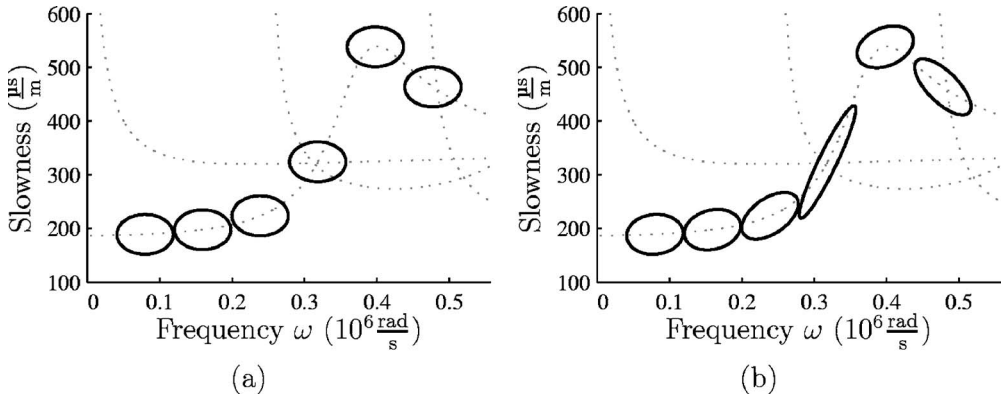

FIG. 7. (a) Regions over which time-frequency content is averaged when evaluating the spectrogram on the dispersion curve of mode s_0. (b) Time-sheared chirplets, concentrated along the dispersion curve of the s_0 mode.

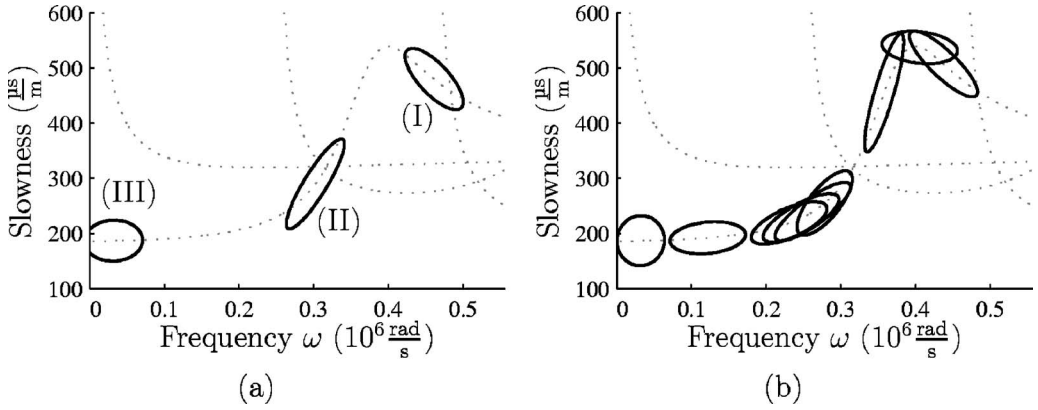

FIG. 9. Region of influence of chirplets concentrated along the s_0 mode. (a) Chirplets interfering (I) with an intersecting dispersion curve, (II) with neighboring and intersecting dispersion curves, and (III) out-of-range chirplet. (b) Adaptive chirplets to avoid interferences.

are generated from a Gaussian window centered on a point on the dispersion curve of the mode under consideration (s_0 or a_0), and time sheared as to be concentrated along the curve. A standard scale s is then chosen analogous to the window length of a STFT. For this work $s=1.3$ rad. Next, the chirplets generated under this procedure are examined to determine whether they interfere with other dispersion curves. As all window functions have an infinite extent (width) in either the frequency or time dimension (or both, like the Gaussian window used in this work), a threshold is applied to the window, under which its value is assumed to be 0. In this research, the finite extent (area) of the Gaussian window is assumed to be 2.8 times the standard deviation, so that 99.9% of the energy of the window is located within this area. With this criteria, an interference is defined as another dispersion curve lying within this 99.9% area.

If the resulting chirplet or its region of averaging interferes with a dispersion curve of another mode, its scaling factor is varied to avoid interferences. This scaling stretches the chirplet in one direction (either time or frequency) and shrinks it reciprocally in the other; this is demonstrated in Fig. 9. No scaling factor, however, can avoid interference for points near the intersection of two dispersion curves, or on portions of a dispersion curve where other dispersion curves are close. In these instances, the energy distribution cannot be calculated properly for the corresponding frequencies, so the chirplet analysis is not performed for these frequencies. Figure 10 indicates the regions of each dispersion curve where these adaptive, interference-free chirplets can be designed. Finally, note that these limitations are directly related to a wave's propagation distance. For a larger propagation distance d, a window with a certain time and frequency extent (area) has a smaller slowness dimension—as slowness is inversely proportional to propagation distance. This implies that, for larger propagation distances, it is easier to fit chirplets on dispersion curves while avoiding interferences. Figure 10 shows these frequency intervals for propagation distances of $d=90$ mm (black lines), and $d=900$ mm (gray lines).

The adaptive chirplet algorithm is applied to the same synthetic Lamb wave signal, and the results are shown in Fig. 11. Since this s_0-mode distribution is normalized to mode a_0, mode displacement ratio values are only calculated in frequency regions where both the s_0 and a_0 energies can be calculated without interference. Figure 11 shows that the chirplet transform is capable of accurately extracting the (proportional) energy distribution of an individual mode from a multimode signal. Normalization to the a_0-mode em-

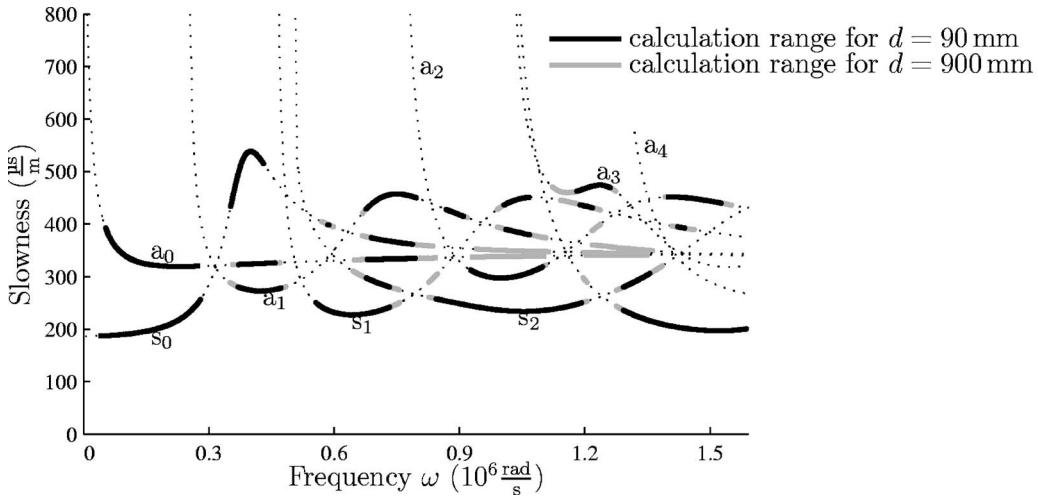

FIG. 10. Dispersion curves (dotted lines), indicating the regions where adaptive chirplets can be applied to the synthetic time signal without interferences with other modes for propagation distance $d=90$ mm (black lines) and $d=900$ mm (gray lines).

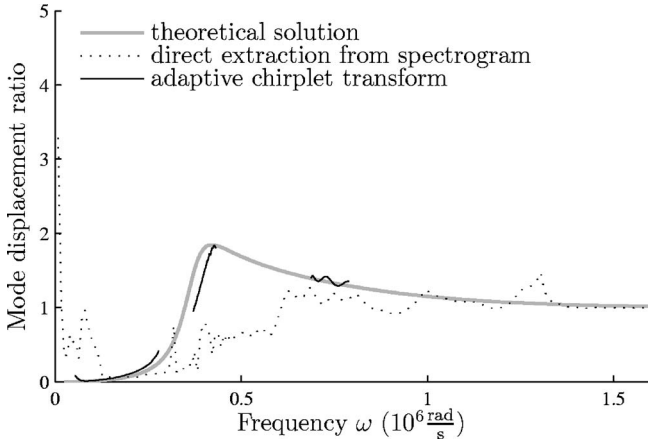

FIG. 11. Mode displacement ratio of mode s_0 over mode a_0, obtained by using adaptive chirplets (solid black line). Results only exist where both a_0 and s_0 modes can be evaluated. Compare to theoretical displacement ratio (solid gray line), and the previously obtained results by directly evaluating the spectrogram (dotted line).

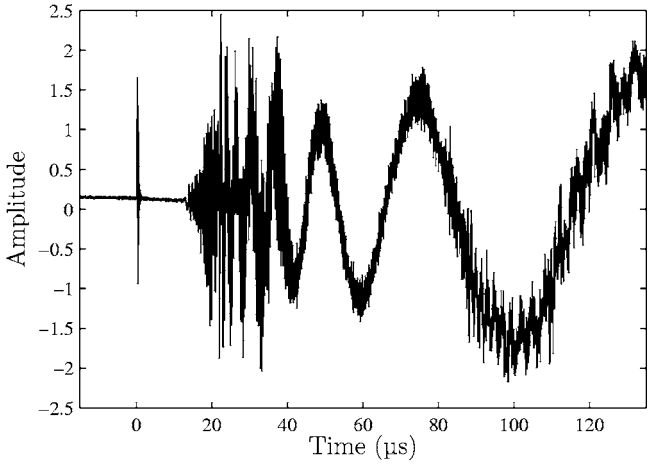

FIG. 12. Typical time-domain signal (out-of-plane particle velocity) measured in the perfect plate.

phasizes small discrepancies, but the computed mode displacement values are very close to the exact (theoretical) values.

The adaptive chirplet algorithm procedure yields a quantitative prediction of the mode energy, and uses the uncertainty principle to identify the slowness-frequency regions where interference will occur. This research takes a conservative approach to identifying these regions, and an advantage of the proposed adaptive algorithm is that the user can quantitatively define the interference criteria for a particular application. For example, a user could specify that certain modes do not exist (or at least do not carry significant energy) for higher frequencies, so no interference will occur with these modes. This would lead to an expanded frequency region in which to calculate energy content; note that this adds credibility to the fact that the energy content for higher frequencies in Fig. 8 is actually correct (but excluded in Fig. 11).

V. APPLICATION TO EXPERIMENTALLY MEASURED SIGNALS

As a final step, the accuracy and robustness of the adaptive chirplet algorithm is demonstrated on real, experimentally measured Lamb wave signals with an application of the correlation technique developed in previous research.[4,10] Benz *et al.*[10] formulated this correlation technique using the reflected Lamb wave field to locate a notch in a 0.99 mm thick, 3003 aluminum plate. These Lamb wave signals are generated with a pulse laser (noncontact, pointlike, broad band generation), and detected with a dual probe laser interferometer (noncontact, high fidelity, pointlike detection) in both a notched and a perfect plate. Figure 12 shows a typical time-domain signal (out-of-plane particle velocity) measured in the perfect plate; note that the spike at $t=0$ is spurious, and corresponds to the firing of the pulse laser. The correlation procedure of Benz *et al.*[10] uses the spectrogram to calculate the energy reflected by the notch in a certain frequency band (300 kHz–2 MHz).

In brief, their technique examines a correlation of the spectrograms measured in a notched plate (known location of this notch is $\Delta d_0' = 29.2$ mm) and in a perfect plate—each calculated with different, assumed propagation distances, $\Delta d_0'$. Reflections (from the notch and any plate edges) will introduce local maxima in the correlation curves at certain propagation distances. These local maxima occur when the reflected modes (within a spectrogram) coincide with the incident modes, which in turn provide a notch (or plate edge) location distance. A ratio of the notched to perfect plate correlations removes the maxima due to plate edges (the edges are present in both notched and plate specimens) and will show maxima only at "reflecting" features that are present in the notched plate, but not in the perfect plate. The notch is the only such feature in these experiments.

Benz[19] notes that the a_0-mode carries a large portion of the energy of a Lamb wave and is less affected by mode conversion at the notch. This implies that correlation calculations should focus on that particular mode, and this goal is achieved in Ref. 10 by restricting the spectrogram calculation to a limited frequency band (namely, 300 kHz–2 MHz).

In contrast, the chirplet transform enables the calculation of the energy of each mode individually, which will be used to formulate an alternative notch localization technique. In a fashion similar to Ref. 10, the adaptive chirplet transform is applied to an experimentally measured time-domain signal for a number of assumed propagation distances, $\Delta d_0'$. In other words, adaptive chirplet analysis is performed on the a_0-dispersion curve in slowness-frequency coordinates according to these propagation distances. This results in energy distributions over frequency for each distance. Instead of correlating spectrogram images (as in Ref. 10), the correlation of energy distributions of mode a_0 for varying assumed propagation distances is calculated.

Figure 13 shows two ratio curves (ratio of the correlations of the notched to perfect plates). One ratio curve is determined with the adaptive chirplet algorithm developed in this research, while the other curve is based on the reassigned spectrograms as described by Benz *et al.*[10] Both algorithms lead to very accurate notch localization—they both contain peaks at the correct notch location distance of $\Delta d_0'$

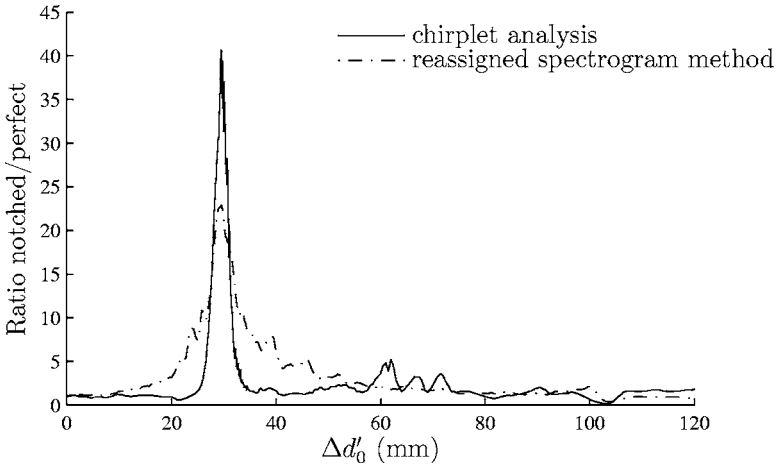

FIG. 13. Ratio curves for notch localization performed with a correlation method based on the reassigned spectrogram and the adaptive chirplet algorithm, respectively.

=29.2 mm to within ±0.4 mm, an error of 1%. However, the ratio curve calculated with the adaptive chirplet algorithm has a peak that is much sharper and higher, providing a more definitive indication of the notch location.

VI. CONCLUSION

This research demonstrates the effectiveness of using the chirplet transform as a signal processing tool to quantitatively determine the energy distribution of the individual modes of a multimode, dispersive Lamb wave. The proposed adaptive chirplet algorithm is grounded in the theory developed by Mann,[5] and is model-based; this work uses a model of the dispersion relationship (the Rayleigh-Lamb equations) to assign wave energy to the individual propagation modes by fitting chirplets to these known modelines. An adaptive algorithm then quantitatively determines the frequency regions (for each mode) in which reliable calculations of mode energy are possible, and employs chirplets (locally adapted) to extract the (proportional) energy distribution of that mode from a dispersive, time-domain wave signal.

This adaptive chirplet algorithm is first validated on a synthetic Lamb wave signal (time-domain, multimode, dispersive), and shows its effectiveness and accuracy for the quantitative measurement of mode energy content.

The robustness of this adaptive chirplet algorithm is then demonstrated on experimentally measured Lamb wave signals. This application enables a demonstration of another advantage of the proposed adaptive chirplet algorithm—the ability to tailor the chirplet atoms to a particular mode, contained within a multimode signal. The correlation procedure developed by Benz *et al.*[10] is modified for the chirplet algorithm and used to locate a notch in a plate with a high degree of accuracy and confidence.

ACKNOWLEDGMENTS

The Deutscher Akademischer Austausch Dienst (DAAD) provided partial support to Helge Kuttig. The National Science Foundation provided partial support to Laurence J. Jacobs under Grant No. CMS-0201283.

[1]D. E. Chimenti, "Guided waves in plates and their use in materials characterization," Appl. Mech. Rev. **50**, 247–284 (1997).
[2]M. Niethammer, L. J. Jacobs, J. Qu, and J. Jarzynski, "Time-frequency representation of Lamb waves," J. Acoust. Soc. Am. **109**, 1841–1847 (2001).
[3]S. Hurlebaus, L. Gaul, and L. J. Jacobs, "Localization of a 'synthetic' acoustic emission source on the surface of a fatigue specimen," Res. Nondestruct. Eval. **13**, 105–117 (2001).
[4]S. Hurlebaus, M. Niethammer, L. J. Jacobs, and C. Valle, "Automated methodology to locate notches with Lamb waves," ARLO **2**, 97–102 (2001).
[5]S. Mann and S. Haykin, "The chirplet transform: A generalization of Gabor's logon transform," Vision Interface **91**, 205–212 (1991).
[6]R. G. Baraniuk and D. L. Jones, "Wigner-based formulation of the chirplet transform," IEEE Trans. Signal Process. **44**, 3129–3135 (1996).
[7]S. Mann and S. Haykin, "The chirplet transform: Physical considerations," IEEE Trans. Signal Process. **43**, 2745–2761 (1995).
[8]R. Gribonval, "Fast matching pursuit with a multiscale dictionary of Gaussian chirps," IEEE Trans. Signal Process. **49**, 994–1001 (2001).
[9]J.-C. Hong, K. H. Sun, and Y. Y. Kim, "Dispersion-based short-time Fourier transform applied to dispersive wave analysis," J. Acoust. Soc. Am. **117**, 2949–2960 (2005).
[10]R. Benz, M. Niethammer, S. Hurlebaus, and L. J. Jacobs, "Localization of notches with Lamb waves," J. Acoust. Soc. Am. **114**, 677–685 (2003).
[11]O. Kotte, M. Niethammer, and L. J. Jacobs, "Lamb wave characterization by differential reassignment and nonlinear anisotropic diffusion," NDT & E Int. **39**, 96–105 (2006).
[12]S. Mallat, *A Wavelet Tour of Signal Processing* (Academic, New York, 1999).
[13]L. Cohen, *Time-Frequency Analysis* (Prentice-Hall, New Jersey, 1995).
[14]The Wigner-Ville distribution does not result in any smoothing of the time-frequency representation, but is not guaranteed to be positive and suffers from signal interferences.
[15]J. D. Achenbach, *Wave Propagation in Elastic Solids* (Elsevier, New York, 1973).
[16]R. L. Weaver and Y. H. Pao, "Axisymmetric elastic waves excited by a point source in a plate," Trans. ASME, J. Appl. Mech. **49**, 821–836 (1982).
[17]P. Wilcox, "Modelling the excitation of Lamb and SH waves by point and line sources," in *Review of Progress in Quantitative Nondestructive Evaluation*, edited by D. O. Thompson and D. E. Chimenti, AIP Conf. Proc. (AIP, New York, 2004), Vol. **23A**, pp. 206–213.
[18]H. Kuttig, "Model-based signal processing of dispersive waves with chirplets," Diplomarbeit thesis, Institute A for Mechanics, University of Stuttgart (2005).
[19]R. Benz, "Localization of notches with Lamb waves," Master thesis, School of Civil and Environmental Engineering, Georgia Institute of Technology (2002).